REnal Flow and Microstructure AnisotroPy (REFMAP) MRI in Normal and Peritumoral Renal Tissue

Andrea L. Liu, BA,[1]* Artem Mikheev, BS,[2,3] Henry Rusinek, PhD,[2,3] William C. Huang, MD,[4] James S. Wysock, MD, MS,[4] James S. Babb, PhD,[2,3] Thorsten Feiweier, PhD,[5] David Stoffel, BS,[2,3] Hersh Chandarana, MD,[2,3] and Eric E. Sigmund, PhD[2,3]

Background: Diffusion-weighted imaging (DWI) provides insight into the pathophysiology underlying renal dysfunction. Variants of DWI include intravoxel incoherent motion (IVIM), which differentiates between microstructural diffusion and vascular or tubular flow, and diffusion tensor imaging (DTI), which quantifies diffusion directionality.
Purpose: To investigate the reproducibility of joint IVIM-DTI and compare controls to presurgical renal mass patients.
Study Type: Prospective cross-sectional.
Subjects: Thirteen healthy controls and ten presurgical renal mass patients were scanned. Ten controls were scanned twice to investigate reproducibility.
Field Strength/Sequence: Subjects were scanned on a 3T system using 10 b-values and 20 diffusion directions for IVIM-DTI in a study approved by the local Institutional Review Board.
Assessment: Retrospective coregistration and measurement of joint IVIM-DTI parameters were performed.
Statistical Analysis: Parameter reproducibility was defined as intraclass correlation coefficient (ICC) >0.7 and coefficient of variation (CV) <30%. Patient data were stratified by lesion side (contralateral/ipsilateral) for comparison with controls. Corticomedullary differentiation was evaluated.
Results: In controls, the reproducible subset of REnal Flow and Microstructure AnisotroPy (REFMAP) parameters had average ICC = 0.82 and CV = 7.5%. In renal mass patients, medullary fractional anisotropy (FA) was significantly lower than in controls (0.227 ± 0.072 vs. 0.291 ± 0.044, $P = 0.016$ for the kidney contralateral to the mass and 0.228 ± 0.070 vs. 0.291 ± 0.044, $P = 0.018$ for the kidney ipsilateral). In the kidney ipsilateral to the mass, cortical $D_{p,radial}$ was significantly higher than in controls ($P = 0.012$). Conversely, medullary $D_{p,axial}$ was significantly lower in contralateral than ipsilateral kidneys ($P = 0.027$) and normal controls ($P = 0.044$).
Data Conclusion: REFMAP-MRI parameters provide unique information regarding renal dysfunction. In presurgical renal mass patients, directional flow changes were noted that were not identified with IVIM analysis alone. Both contralateral and ipsilateral kidneys in patients show reductions in structural diffusivities and anisotropy, while flow metrics showed opposing changes in contralateral vs. ipsilateral kidneys.
Level of Evidence: 2
Technical Efficacy: Stage 2

J. MAGN. RESON. IMAGING 2018;48:188–197.

Renal disease is one of the most common and impactful diseases worldwide, with the US prevalence of chronic kidney disease (CKD) being 14% in 2012.[1] In current clinical practice, the standard assessment of renal function is estimated glomerular filtration rate (eGFR), which is calculated from serum creatinine levels. However, despite its utility as a low-cost and widely accessible estimate of renal function, eGFR does not assess the laterality of dysfunction,

View this article online at wileyonlinelibrary.com. DOI: 10.1002/jmri.25940

Received Sep 13, 2017, Accepted for publication Dec 14, 2017.

*Address reprint requests to: A.L.L., 660 First Ave., New York, NY 10016. E-mail: andrea.liu@med.nyu.edu

From the [1]New York University School of Medicine, New York, New York, USA; [2]Bernard and Irene Schwartz Center for Biomedical Imaging, Department of Radiology, New York University School of Medicine, New York, New York, USA; [3]Center for Advanced Imaging and Innovation (CAI[2]R), New York University School of Medicine, New York, New York, USA; [4]Department of Urology, New York University School of Medicine, New York, New York, USA; and [5]Siemens Healthcare GmbH, Erlangen, Germany

differentiate pathophysiology, or predict recovery. The equations in current use overestimate eGFR in patients with comorbid liver disease,[2] and have poor accuracy in populations with renal dysfunction but normal eGFR; for example, early in the course of diabetes.[3,4]

Given the limitations of the established measures of renal function, there is a potential role for imaging. However, most radiologists follow a serum creatinine threshold beyond which they will not administer contrast for CT.[5] Dynamic contrast-enhanced (DCE) magnetic resonance imaging (MRI) has been shown to provide information on renal function,[6,7] but its use is limited in populations with renal insufficiency.[8] Many patients with renal masses have preexisting renal dysfunction; for example, in one retrospective cohort study, 26% of patients who received either a partial or radical nephrectomy had preoperative CKD.[9]

The pathophysiology underlying renal dysfunction is a complex interplay of microstructural and microvascular phenomena. Diffusion-weighted imaging (DWI) techniques have attempted to describe the complexities of renal tissue.[10] Intravoxel incoherent motion (IVIM) is a DWI technique that uses biexponential fitting of signal acquired over a range of b-values to differentiate between microstructural diffusion and vascular or tubular flow (pseudodiffusion).[11] In renal allograft patients, IVIM measures are sensitive to rejection.[12] In renal mass patients these measures provide information about tumor subtype and vascularity.[13,14]

Another variant of DWI is diffusion tensor imaging (DTI), which uses an anisotropic Gaussian matrix description to quantify the directionality of diffusion.[15] As tubules, arterioles, and venules in a healthy kidney are oriented radially, the kidney is anisotropic on DTI.[16,17] Renal diffusion anisotropy has been previously shown to decrease with diabetic nephropathy,[18] allograft dysfunction,[19,20] ischemia-reperfusion damage (in a rat model),[21] and impaired renal function with other causes.[22]

A previous study had demonstrated a joint IVIM-DTI methodology to assess the directionality of both the pseudodiffusion and tissue diffusion components of water motion anisotropy.[23] That work suggested that both tubular/vascular flow and diffusion play a role in medullary anisotropy.[23] Several other recent studies have also explored renal imaging sequences that combine differentiation between flow and diffusion with measures of anisotropy.[24,25]

The purpose of this study was to investigate the reproducibility of joint intravoxel incoherent motion-diffusion tensor imaging (IVIM-DTI) and compare controls to presurgical renal mass patients. We hypothesized that differentiating between perfusion and diffusion when quantifying anisotropy will contribute to our understanding of renal function as seen in DWI, as distinguishing between components of water transport may be able to help differentiate renal damage from changes in flow and eventually play a role in outcome prediction.

Materials and Methods

Subjects

This Health Insurance Portability and Accountability Act-compliant study was approved by the Institutional Review Board. Written informed consent was obtained from all subjects. Subjects were instructed to abstain from consumption of caffeine for 3 hours before image acquisition. Thirteen volunteers (six male and seven female, ages 26–63 years with mean 39.5 ± 12.6 years, body mass index (BMI) 20.8–39.9 with mean 27.3 ± 6.1) without known renal dysfunction were recruited for this study. A subset of 10 of the volunteers (three male and seven female, ages 26–63 years with mean 40.2 ± 13.3 years, BMI 20.8–39.9 with mean 26.9 ± 6.6) were each imaged twice at a mean interval of 39.4 ± 31.7 days, with a minimum interval of 2 days and maximum interval of 93 days. Eleven patients who had previous imaging suspicious for renal cell carcinoma (RCC) were recruited from urology patients scheduled for clinically indicated renal MRI. One patient was excluded from analysis, as clinical MRI was read as angiomyolipoma (benign lesion). The renal mass patients (eight male and two female, ages 34–80 years with mean 61.4 ± 13.0 years, BMI 22.4–36.8 with mean 28.8 ± 5.6) were surgical candidates imaged preoperatively. Patient eGFR calculated with the Modification of Diet in Renal Disease (MDRD) formula ranged from 12.3–181.6 with mean 81.5 ± 49.7. At the time of this report, four patients had proceeded to partial nephrectomy. Mass subtype was clear-cell RCC for two patients with 19% and 28% postoperative eGFR reduction, clear cell papillary RCC with no postoperative change in eGFR for one patient, and one patient had nephrectomy performed at an outside institution.

Imaging Protocol

All imaging was performed on a clinical wide-bore 3T scanner (Magnetom Skyra, Siemens Healthcare, Erlangen, Germany) using a 6-element body array matrix coil and 12 elements of the integrated spine coil. T_2-weighted half-Fourier acquisition single-shot turbo spin-echo (HASTE) oblique coronal images (repetition time [TR] 1200 msec; echo time [TE] 91 msec; matrix 320×256; voxel size $1.1 \times 1.1 \times 5\,mm^3$) were acquired for morphology and planning. IVIM-DTI acquisitions were performed during free-breathing using a prototype twice-refocused spin-echo echo-planar-imaging (TRSE-EPI) sequence with spectrally adiabatic inversion recovery (SPAIR), reversed slice gradient polarity fat suppression, and additional spoiling[26] (parameters: TR 2600 msec; TE 74 msec; matrix 192×180; voxel size $2.2 \times 2.2 \times 6\,mm^3$; b-values 0, 10, 30, 50, 80, 120, 200, 400, 600, 800 s/mm^2; 20 diffusion directions for all nonzero b-values; 2 averages; 5 to 8 slices). DWI were acquired in an oblique coronal orientation with the readout direction along the long axis of the kidney as indicated in localizer and HASTE imaging. Inline correction of eddy-current-induced distortion was performed on the vendor workstation. IVIM-DTI sequence acquisition time was 15 minutes.

Data Analysis

To correct for respiratory kidney motion and to achieve more accurate cortex/medulla segmentation, the kidneys on EPI images of each patient were coregistered. In order to account for the different respiratory motion trajectory of left and right kidney, coregistration was performed separately for each kidney.[27] Affine 2D registration used mutual information criterion as a similarity measure. After motion correction, images were visually screened by one investigator for registration accuracy and consistent signal intensity. A median (nonlinear edge preserving) filter of 3 × 3 voxels was then applied to all aligned images. IVIM-DTI analysis (described below) was performed with custom code (Igor Pro, Wavemetrics, Portland, OR). For each slice, one investigator defined regions of interest (ROIs) on all slices, using the b = 0 (b_0) image for the cortex and on the fractional anisotropy (FA) map for the medulla. Renal masses were excluded in patients; otherwise, ROIs were placed over the entire cortex and medulla.

Signal-to-noise ratio (SNR) in each kidney was estimated using image subtraction.[28] After subtracting images with the same b-value and direction, the mean of the voxelwise standard deviations over an ROI was used as an estimate of the image noise after division by the square root of 2. The SNR for each pair of averages was taken to be the mean signal intensity divided by the estimated noise over an ROI drawn on the whole kidney. Average SNR for each b-value was calculated over all directions for each subject, and subject group averages and standard deviations computed.

IVIM-DTI Analysis

IVIM and DTI analyses were first both performed separately, in accordance with conventional approaches.[11,15] For combined IVIM-DTI analysis, as previously described by Notohamiprodjo et al, a cylindrical two-compartment model was used to quantify the global anisotropies of the diffusion and perfusion components.[23] First, IVIM analysis was performed voxelwise using a segmented biexponential fit[11]:

$$\frac{M}{M_0} = f_p e^{-bD_p} + (1-f_p)e^{-bD_t} \quad (1)$$

where M is magnetization, M_0 total magnetization, f_p perfusion fraction, D_p pseudodiffusivity, and D_t tissue diffusivity. Using the assumption that $e^{-bD_p} \to 0$ if the b-value is sufficiently large (assumed to be sufficient at b >200 s/mm^2), Eq. 1 simplifies to:

$$\frac{M}{M_0} = (1-f_p)e^{-bD_t} \quad (2)$$

D_t was determined by monoexponential fit to Eq. 2 at b-values >200 s/mm^2. f_p was then determined as:

$$f_p = \frac{M_0 - M_{\text{intercept}}}{M_0} \quad (3)$$

where $M_{intercept} = M_0(1-f_p)$ is the zero intercept. Finally, D_p was determined by fitting Eq. 1 for all b-values with the previously determined D_t and f_p.

Next, DTI analysis was performed. A 3 × 3 symmetric diffusion tensor with eigenvectors $(\vec{v}_1, \vec{v}_2, \vec{v}_3)$ and eigenvalues $(\lambda_1,\lambda_2,\lambda_3)$ was fitted to the D_t values obtained in the IVIM analysis.[15,29] The scalar perfusion fraction $f_{p,scalar}$ was fixed as the average perfusion fraction over all directional values $f_{p,avg}$. For each gradient direction, a second IVIM fit was then performed to determine directional D_p values, using the corresponding D_t for each direction and fixed $f_{p,scalar}$ for all directions.

Separately for the cortical and medullary ROIs of a selected central slice, D_t and D_p from all voxels were "projected" along the primary tensor axis.[30,31] The polar angle $\theta = \cos^{-1}(\vec{g} \cdot \vec{v}_1)$ between the corresponding diffusion gradient $\vec{g}$ and the tensor direction, represented by the primary eigenvector $\vec{v}_1$, was used to plot the D_t and D_p values for all directions. Separately for cortical and medullary ROIs, all voxels were divided by polar angle into 40 bins in the range $0 < \theta < 180°$. Consistent with the cylindrically symmetric description, data at each polar angle was reflected into each quadrant of the polar plane. The mean and standard error of all D_t and D_p values were calculated in each bin for the resulting oversampled dataset. A quadratic fit $D_t = D_{t,axial} + (D_{t,axial} - D_{t,radial})\cos^2\theta$ was performed with values from the averaged angular distribution[15] to determine global tissue diffusivity along the axial $(\vec{v}_1)$ and radial (perpendicular to $\vec{v}_1$) directions $D_{t,axial}$ and $D_{t,radial}$. An equivalent fit was performed to determine global pseudodiffusivity parameters $D_{p,axial}$ and $D_{p,radial}$.

Mean diffusion MD and fractional anisotropy for each compartment were then estimated from the DTI eigenvalues:

$$MD = \frac{1}{3}(\lambda_1 + \lambda_2 + \lambda_3) \quad (4)$$

$$FA = \sqrt{\frac{3}{2}}\sqrt{\frac{(\lambda_1 - MD)^2 + (\lambda_2 - MD)^2 + (\lambda_3 - MD)^2}{\lambda_1^2 + \lambda_2^2 + \lambda_3^2}} \quad (5)$$

where FA is fractional anisotropy and MD mean diffusivity. Analogously, assuming cylindrical symmetry, ie, $\lambda_2 = \lambda_3$,[10] global structural mean diffusivity MD_t and fractional anisotropy FA_t were estimated:

$$MD_t = \frac{1}{3}(D_{t,\text{axial}} + 2D_{t,\text{radial}}) \quad (6)$$

$$FA_t = \sqrt{\frac{3}{2}}\sqrt{\frac{(D_{t,\text{axial}} - MD_t)^2 + 2(D_{t,\text{radial}} - MD_t)^2}{D_{t,\text{axial}}{}^2 + 2D_{t,\text{radial}}{}^2}} \quad (7)$$

with equivalent calculations to estimate MD_p and FA_p. This parameter set is termed Renal Flow and Microstructure AnisotroPy (REFMAP)-MRI.

Statistical Analysis

Reproducibility analysis was performed using the 10 control subjects who provided data on two separate dates. Restricted maximum likelihood estimation of variance components in a random effects model was used to estimate the intra- and intersubject components of the overall variance in each regional measure. The estimated components were used to compute the intraclass correlation (ICC) and intrasubject coefficient of variation (CV) as estimates of

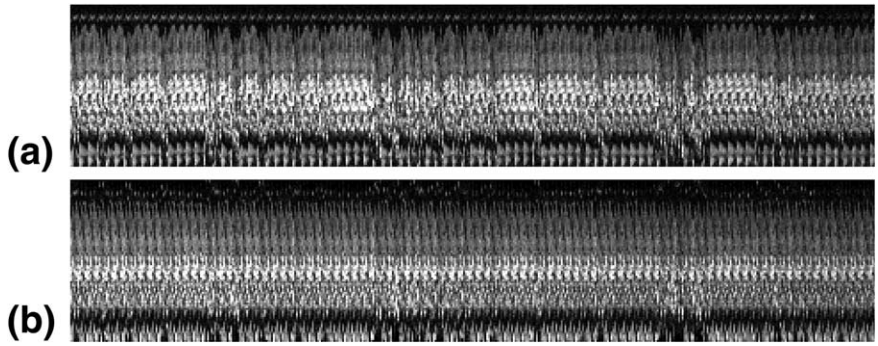

FIGURE 1: Time series of sagittal 1D line profiles through the center of a lesion-bearing kidney in a presurgical renal mass patient, showing postacquisition 2D affine registration. Preregistration images (a) demonstrate cyclical respiratory motion, which is dramatically reduced in the postregistration images (b).

the repeatability of each measure. A Bland–Altman analysis to assess agreement between results from the two visits was used to determine the limits of agreement (LoA) and mean additive bias of each regional measure. An exact Wilcoxon signed-rank test was used to assess whether the within-subject difference between visits was significantly different from 0; a significant result would imply significant mean additive bias.

For quality control and comparison with lesion-bearing patients, laterality analysis was performed on the 13 volunteers without renal masses, using the first exam only for volunteers who were scanned twice. An exact Wilcoxon signed-rank test was used to assess whether the within-subject difference between the left and right kidneys was different from 0.

Weighted analysis of variance (ANOVA) was used to compare the regional measures on the contralateral and ipsilateral sides of patients to the regional measures of controls. Since the concept of contralateral and ipsilateral sides does not extend to controls, each regional measure was represented for each control subject as an average over the left and right kidneys using the data from the first visit. To account for the fact that control data were represented as an average over kidneys, whereas patients provided data for each individual kidney, the data were weighted according to the number of observations each value represented. All statistical tests were conducted at the two-sided 5% significance level using SAS 9.3 software (SAS Institute, Cary, NC).

Results

All examinations were of sufficient quality for analysis after motion correction and screening of individual images by visual inspection; no kidney was excluded from analysis. Time series showing example results of retrospective 2D affine registration via sagittal line profiles through a patient kidney are given in Fig. 1. In healthy volunteers, overall 2.10% of images were excluded based on image quality and registration success. In renal mass patients, overall 3.03% of images were excluded. For healthy volunteers, SNR before averaging ranged from 11.94 averaged across images with $b = 0$ s/mm^2 to 5.63 across $b = 800$ s/mm^2. In renal mass patients, SNR ranged from 9.58 averaged across images with $b = 0$ s/mm^2 to 3.55 across $b = 800$ s/mm^2.

For the healthy volunteers who were scanned on 2 separate days, the only parameter with significant intrasubject variance was medullary $D_{t,radial}$ ($P = 0.032$). ICC and CV of all IVIM, DTI, and combined IVIM-DTI analyses are summarized in Table 1, with the subset of reproducible parameters defined as ICC >0.7 and CV <30%, as shown in Fig. 2. Among structural parameters, λ_1, λ_2, λ_3, MD/D_t, and FA meet this reproducibility criteria. Among flow parameters, f_p, MD_p (medulla only), D_p (medulla only), and $D_{p,axial}$ (medulla only) meet this reproducibility criteria.

Laterality analysis in volunteers without renal masses showed significant differences only for medullary $D_{p,radial}$ ($P = 0.030$, left mean = 26.49 * 10^{-3} mm^2/s, right mean = 19.14 * 10^{-3} mm^2/s), cortical $D_{t,axial}$ ($P = 0.012$, left mean = 2.37 * 10^{-3} mm^2/s, right mean = 2.26 * 10^{-3} mm^2/s), and cortical $D_{t,radial}$ ($P = 0.017$, left mean = 1.89 * 10^{-3} mm^2/s, right mean = 1.81 * 10^{-3} mm^2/s).

Data for the separate IVIM, DTI, and combined IVIM-DTI analyses for healthy volunteers and renal mass patients are summarized in Table 2, with example maps shown in Fig. 3. In control kidneys, all structural parameters (λ_1, λ_2, λ_3, MD, FA, D_t, $D_{t,axial}$, $D_{t,radial}$, MD_t, FA_t) and some flow parameters (f_p, $D_{p,axial}$, FA_p) showed significant corticomedullary differentiation.

In both the kidney contralateral to and ipsilateral to the mass, mean medullary FA was significantly lower than in controls ($P = 0.016$ and $P = 0.018$, respectively) (Fig. 4). In both patient kidneys, medullary λ_1, $D_{t,axial}$, and FA_t were significantly lower than in controls ($P = 0.017$, $P = 0.007$, $P = 0.005$ for the contralateral kidney; $P = 0.034$, $P = 0.049$, $P = 0.022$ for the ipsilateral kidney). In the kidney ipsilateral to the mass, cortical $D_{p,radial}$ and MD_p were significantly higher than in controls ($P = 0.012$ and $P = 0.018$, respectively). In the kidney contralateral to the mass, medullary $D_{p,axial}$ was significantly lower than in controls ($P = 0.044$). In patients, medullary $D_{p,axial}$ was significantly higher in the ipsilateral than the contralateral kidney ($P = 0.027$). Exemplary polar plots showing D_t and D_p "projected" along the structural primary tensor axis are

TABLE 1. Intervisit Reproducibility Measures for IVIM, DTI, and Combined IVIM-DTI Analysis

	Cortex			Medulla		
	ICC	CV (%)	Limits of agreement	ICC	CV (%)	Limits of agreement
D_p	0.44	16.1	(−13.38, 7.52)	0.70	23.4	(−21.14, 13.40)
f_p	0.69	14.1	(−7.45, 8.36)	0.80	11.6	(−2.96, 6.08)
MD	0.83	2.1	(−0.128, 0.124)	0.88	2.5	(−0.09, 0.16)
FA	0.77	6.8	(−0.03, 0.03)	0.91	5.3	(−0.03, 0.05)
λ_1	0.75	2.5	(−0.17, 0.17)	0.84	3.7	(−0.19, 0.31)
λ_2	0.83	2.2	(−0.13, 0.12)	0.93	2.1	(−0.075, 0.117)
λ_3	0.89	2.0	(−0.106, 0.104)	0.96	1.8	(−0.063, 0.090)
$D_{t,\ axial}$	0.69	2.8	(−0.19, 0.20)	0.73	4.9	(−0.22, 0.41)
$D_{t,\ radial}$	0.77	2.6	(−0.10, 0.16)	0.87	3.1	(−0.06, 0.15)
MD_t	0.78	2.3	(−0.10, 0.15)	0.76	3.6	(−0.09, 0.22)
FA_t	0.57	14.5	(−0.06, 0.04)	0.88	7.6	(−0.06, 0.07)
$D_{p,\ axial}$	0.59	25.1	(−23.35, 17.39)	0.82	24.8	(−28.55, 30.29)
$D_{p,\ radial}$	0.33	28.5	(−19.52, 17.71)	0.62	35.9	(−21.69, 26.56)
MD_p	0.47	24.3	(−18.76, 15.57)	0.73	29.3	(−22.78, 26.60)
FA_p	0.23	60.6	(−0.29, 0.36)	0.33	37.9	(−0.35, 0.41)

ICC = intraclass correlation coefficient; CV = coefficient of variation.
D_t is constrained to be equivalent to MD and is thus omitted from this table.

shown for a healthy volunteer (Fig. 5) and a patient (Fig. 6).

Corticomedullary differentiation for λ_1 and FA_p was lost in both the ipsilateral ($P = 0.131$ and $P = 0.064$, respectively) and contralateral ($P = 0.492$ and $P = 0.232$) patient kidneys, when compared to controls ($P < 0.001$ and $P < 0.001$). Corticomedullary differentiation for f_p was lost in the ipsilateral patient kidney only ($P = 0.275$), in comparison to controls (0.013). Corticomedullary differentiation for $D_{t,axial}$ and $D_{p,axial}$ was lost in the contralateral patient kidney only ($P = 0.084$ and $P = 0.922$), in comparison to controls ($P < 0.001$ and 0.005). Corticomedullary differentiation for $D_{p,radial}$ was not significant in controls ($P = 0.839$) but was significant in patient contralateral kidneys ($P = 0.020$).

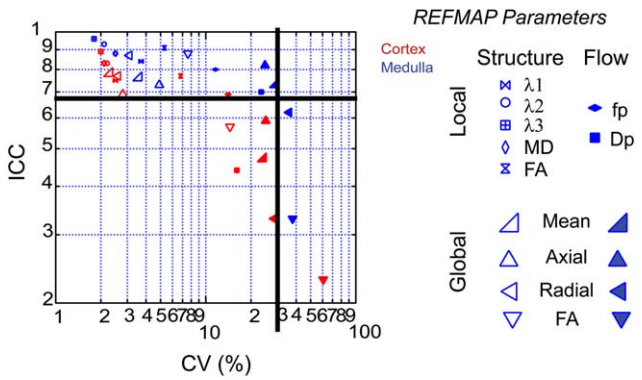

FIGURE 2: Reproducibility metrics for REFMAP-MRI biomarkers of healthy volunteer kidneys. The subset of robust parameters is defined as those with ICC >0.7 and CV <30%. These thresholds are indicated by bold lines.

Discussion

This study performed reproducibility analysis using a recently developed combined IVIM-DTI protocol, and extended analysis to patients with renal masses. Across all b-values, SNR was sufficient for analysis. On average, the SNR for the patient data was lower than the control data, and more images were manually excluded on the basis of either qualitative signal strength or registration failure, perhaps related to body habitus or patient motion.[32]

The range of diffusion and perfusion parameters observed in this study was generally consistent with the literature, in the context of variability introduced by sample size and physiologic differences.[10,17,23,33] We identified for further focused use in clinical populations a subset of reproducible parameters, including the full structural tensor, cortical and medullary perfusion fraction f_p, and medullary average and global axial pseudodiffusion D_p.

Laterality analysis in controls suggested that the majority of parameters did not differ between the right and left kidneys, with the exception of significantly higher medullary

TABLE 2. REFMAP-MRI Parameters Obtained From Combined IVIM-DTI Analysis Projected Along Axial and Radial Tensor Axis

	Control		Contralateral (CL) Mass		Ipsilateral (IL) Mass		*P*-values					
	Cortex	**Medulla**	**Cortex**	**Medulla**	**Cortex**	**Medulla**	**CL vs. control (cortex)**	**CL vs. control (medulla)**	**IL vs. control (cortex)**	**IL vs. control (medulla)**	**CL vs. IL (cortex)**	**CL vs. IL (medulla)**
IVIM Only												
D_t	2.00 ± 0.10	1.95 ± 0.13[a]	1.96 ± 0.20	1.84 ± 0.22[a]	1.95 ± 0.17	1.86 ± 0.22[a]	0.544	0.188	0.467	0.281	0.557	0.432
D_p	23.99 ± 4.56	25.32 ± 8.81	26.27 ± 12.06	24.41 ± 10.12	27.60 ± 6.19	28.57 ± 7.44	0.474	0.817	0.261	0.411	0.193	0.160
f_p	19.54 ± 5.10	17.17 ± 4.19[a]	20.34 ± 4.88	16.45 ± 3.97[a]	18.51 ± 4.10	16.67 ± 3.46	0.711	0.682	0.633	0.776	0.846	0.375
DTI Only												
MD	2.00 ± 0.10	1.95 ± 0.13[a]	1.96 ± 0.20	1.84 ± 0.22[a]	1.95 ± 0.17	1.86 ± 0.22[a]	0.544	0.188	0.467	0.281	0.557	0.432
FA	0.149 ± 0.021	0.291 ± 0.044[a]	0.153 ± 0.048	0.227 ± 0.072[a]	0.141 ± 0.032	0.228 ± 0.070[a]	0.773	**0.016**	0.545	**0.018**	0.492	0.770
λ_1	2.32 ± 0.12	2.61 ± 0.22[a]	2.26 ± 0.24	2.30 ± 0.32	2.24 ± 0.24	2.34 ± 0.36	0.460	**0.017**	0.326	**0.034**	0.492	0.322
λ_2	1.93 ± 0.11	1.72 ± 0.13[a]	1.92 ± 0.20	1.72 ± 0.20[a]	1.91 ± 0.16	1.73 ± 0.19[a]	0.894	0.950	0.737	0.901	0.625	0.695
λ_3	1.74 ± 0.11	1.51 ± 0.12[a]	1.69 ± 0.19	1.51 ± 0.20[a]	1.70 ± 0.15	1.52 ± 0.19[a]	0.409	0.914	0.495	0.890	0.846	0.432
Combined IVIM-DTI												
$D_{t,\ axial}$	2.31 ± 0.12	2.61 ± 0.22[a]	2.20 ± 0.33	2.27 ± 0.33	2.25 ± 0.25	2.37 ± 0.33[a]	0.241	**0.007**	0.502	**0.049**	1.000	0.557
$D_{t,\ radial}$	1.85 ± 0.10	1.63 ± 0.11[a]	1.77 ± 0.27	1.60 ± 0.19[a]	1.82 ± 0.16	1.63 ± 0.15[a]	0.271	0.683	0.744	0.996	0.846	0.846
MD_t	2.00 ± 0.09	1.96 ± 0.12[a]	1.91 ± 0.28	1.82 ± 0.22[a]	1.97 ± 0.19	1.87 ± 0.19[a]	0.239	0.072	0.628	0.258	0.922	0.625
FA_t	0.134 ± 0.030	0.283 ± 0.052[a]	0.131 ± 0.042	0.205 ± 0.064[a]	0.123 ± 0.026	0.221 ± 0.067[a]	0.853	**0.005**	0.459	**0.022**	0.846	0.193
$D_{p,\ axial}$	27.82 ± 4.76	39.91 ± 16.69[a]	23.02 ± 14.38	24.03 ± 11.86	33.28 ± 14.61	46.45 ± 21.98[a]	0.291	**0.044**	0.231	0.392	0.275	**0.027**
$D_{p,\ radial}$	21.12 ± 4.85	22.82 ± 11.16	25.84 ± 12.11	19.95 ± 11.92[a]	30.33 ± 8.62	29.72 ± 15.46	0.179	0.602	**0.012**	0.215	0.432	0.084
MD_p	23.35 ± 3.42	28.52 ± 12.28	24.90 ± 10.88	21.31 ± 8.87	31.31 ± 9.67	35.30 ± 16.86	0.630	0.211	**0.018**	0.238	0.275	0.084
FA_p	0.213 ± 0.095	0.373 ± 0.110[a]	0.187 ± 0.180	0.299 ± 0.168	0.133 ± 0.100	0.268 ± 0.158	0.632	0.222	0.141	0.088	0.625	0.695

P-values for significantly different groups are highlighted in bold.
D_t = tissue diffusivity (10^{-3} mm^2/s); D_p = pseudodiffusivity (10^{-3} mm^2/s); f_p = perfusion fraction (%); MD = mean diffusivity (10^{-3} mm^2/s); FA = fractional anisotropy.
[a]$P < 0.05$ for corticomedullary comparison.

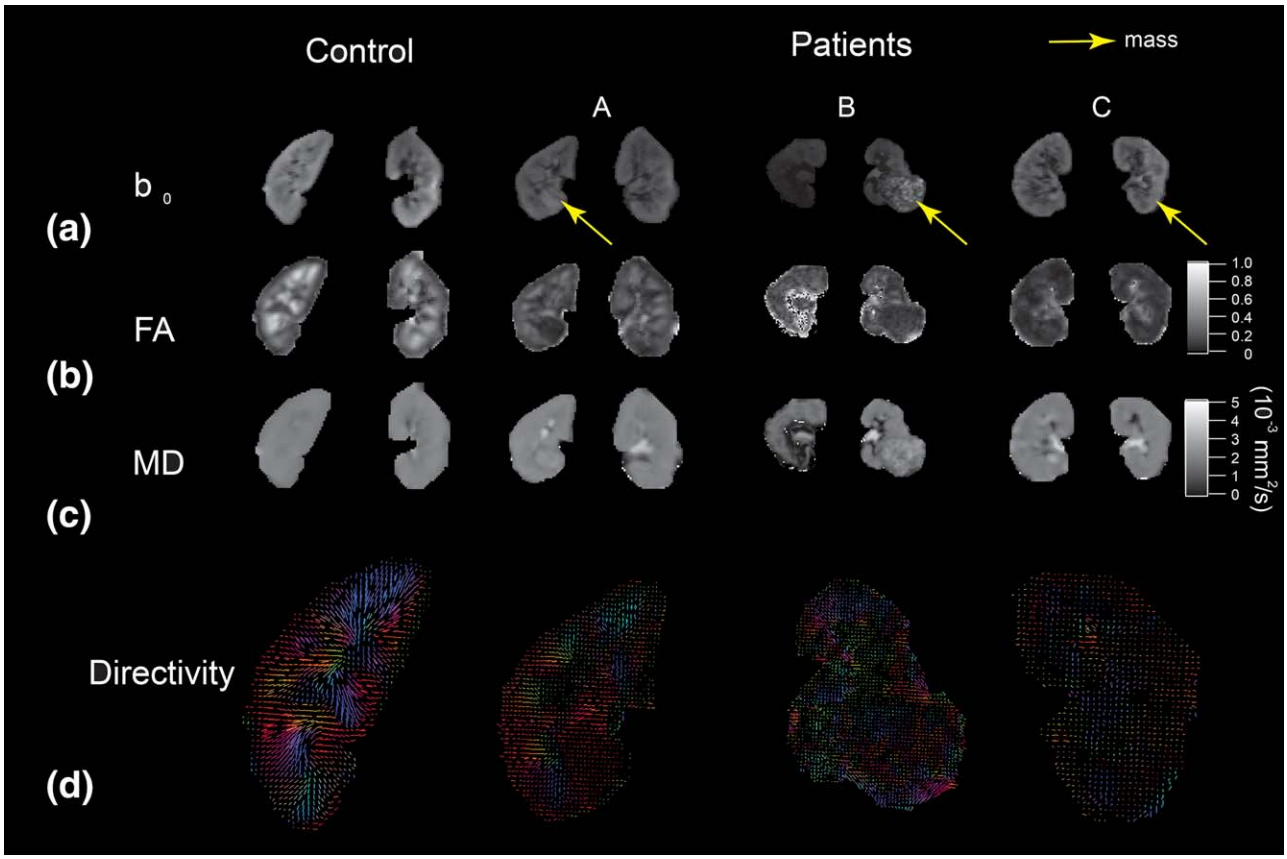

FIGURE 3: Example DTI maps in a healthy volunteer (left) and three patients (right) with renal masses (as indicated by arrows) of varying sizes. b_0 images are shown in (a). Medullary anisotropy is lower (b), mean diffusivity is lower (c), and the pattern of diffusion tensor orientation is more disorganized (d) in the renal mass patients than in the control subject.

radial pseudodiffusion and cortical radial/axial tissue diffusivity in the left kidney. A previous study using a different combined IVIM-DTI approach found significant laterality differences only in cortical f_p, which was higher in the right kidney.[24] These differences may be due to the differing positions, shapes, and sensitivity to the cardiac cycle of the right and left kidneys, and could warrant further investigation, for example for renal transplant planning. Comparison of prone vs. supine subject position may also be informative to exclude scan-related effects. However, none of the baseline laterality differences in controls obstruct our analysis of lesion dependence, as the subsets of parameters significantly differentiating patients from controls do not overlap with those showing laterality in controls, and the effect size in the former tends to exceed that in the latter.

Our analysis of kidneys both contralateral and ipsilateral to renal lesions suggests functional compromise, perhaps reflecting a general deficit that patients have in comparison to controls. Renal ADC has previously been shown to be decreased in the ipsilateral kidney postpartial nephrectomy,[34] as well as in renal artery stenosis[35] and renal failure.[36]

For a range of flow parameters, significant differentiation between the cortex and medulla was lost in renal mass patients, such as the changes in corticomedullary differentiation observed in global axial parameters. In both the ipsilateral and contralateral kidneys, medullary fractional anisotropy was significantly decreased in comparison to the controls, particularly in the axial direction, which may reflect changes in diffusion restriction (such as tissue compression from mass effect) that occur in response to tumor burden. Renal tissue on the side of the renal lesion showed increased flow. The mixed changes observed in the pseudodiffusion parameters may represent tubular flow alterations related to compensatory redistribution of function that occurs as a response to the unilateral presence of a renal lesion. Another possible contributing factor is increased vascularity due to the general tendency of tumors to increase angiogenesis.[37,38] Finally, axial pseudodiffusion $D_{p,axial}$ was the parameter that demonstrated the most lesion dependence. This difference was not apparent with IVIM analysis alone, and serves as an example of the additional information that emerges only with this combined approach that incorporates directionality.

There are several limitations to this study. The sample sizes of controls and renal mass patients were small and inhomogeneous, notably with no measurement of eGFR in controls and with a wide range of renal function in patients. The control and patient populations were not matched, which resulted in differences in factors such as age, sex, and

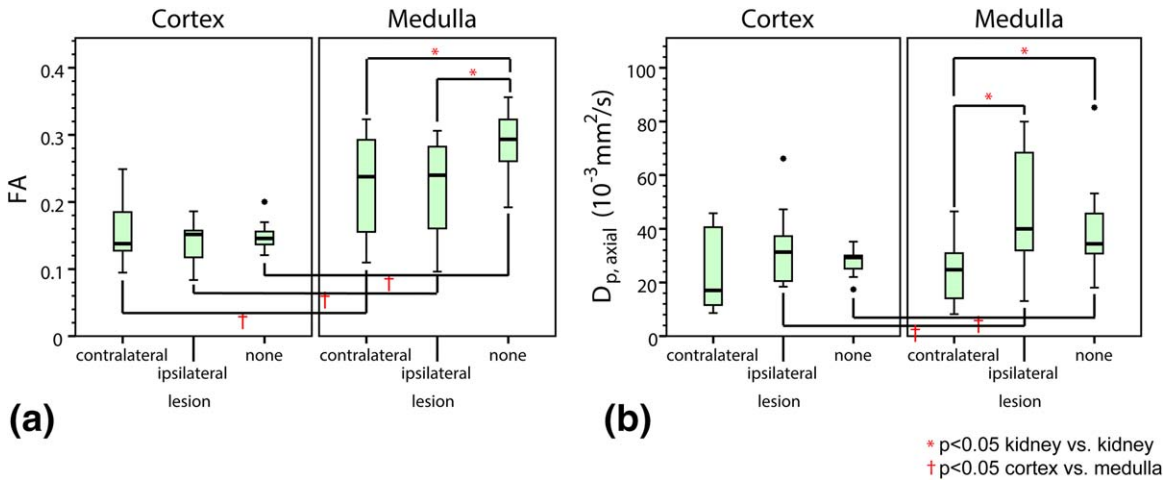

FIGURE 4: Boxplot showing ranges and quartiles for FA and $D_{p,axial}$ in controls (kidneys with no lesion) and renal mass patients (kidneys contralateral and ipsilateral to lesion). FA (a) shows significant corticomedullary differentiation, and medullary values in the patient kidneys (both contralateral and ipsilateral to the lesion) are significantly lower than in controls. Axial medullary pseudodiffusion $D_{p,axial}$ (b) is significantly lower in the patient kidney contralateral to the mass than in controls. When compared to controls, corticomedullary differentiation for $D_{p,axial}$ is lost in the contralateral kidney only.

BMI, which potentially confounded analysis of renal function. In our statistical analysis, we did not correct for multiple comparisons. The acquisition scheme used post-hoc registration rather than respiratory or cardiac gating to minimize scan time, but this may have led to increased variability in flow compartment metrics. Concomitant field

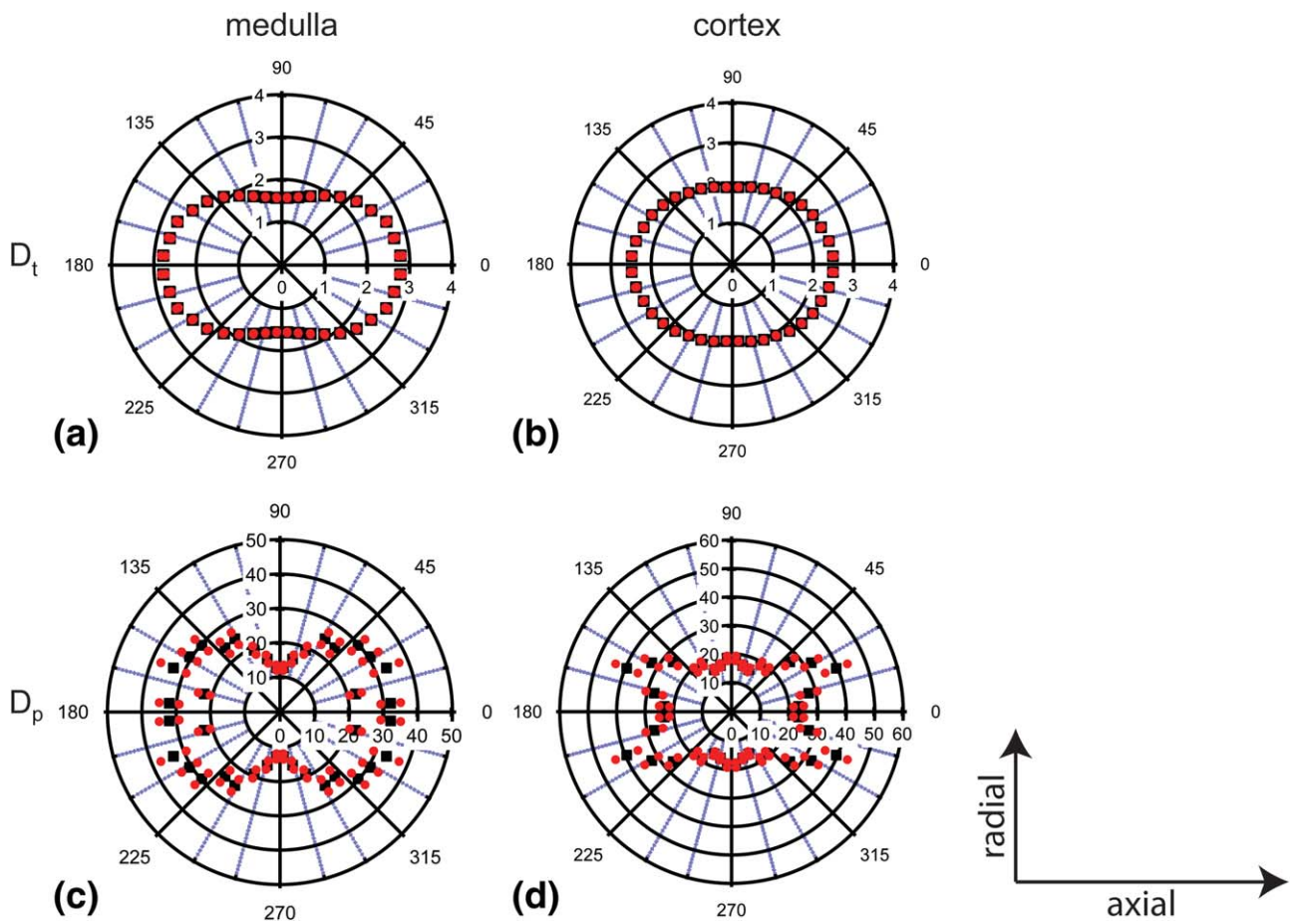

FIGURE 5: Example polar plots in a healthy volunteer, showing the mean (black) and standard error (red) for D_t (a,b) and D_p (c,d) projected along the primary tensor axis. $D_{t,axial}$ is higher and $D_{t,radial}$ lower in the medulla (a) than in the cortex (b). Diffusivities are given in 10^{-3} mm^2/s.

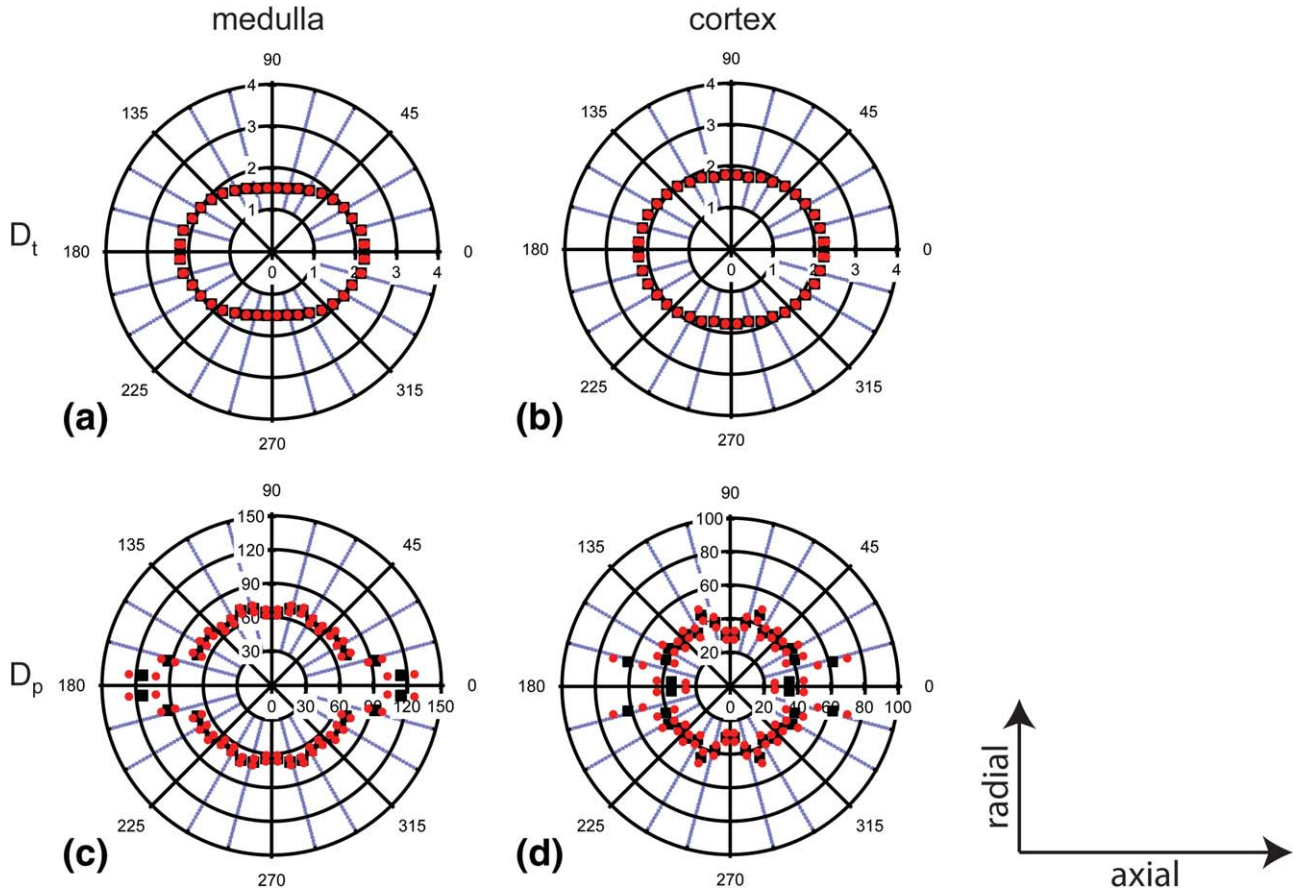

FIGURE 6: Example polar plot for patient kidney ipsilateral to the mass, showing the mean (black) and standard error (red) for D_t (a,b) and D_p (c,d) projected along the primary tensor axis. Compared to control kidneys, medullary anisotropy is decreased. Diffusivities are given in 10^{-3} mm^2/s.

corrections to the diffusion-weighting were not performed but they are expected to be small and uncorrelated with anatomy in this context. The REFMAP quantification scheme includes assumptions (eg, cylindrically symmetric pseudodiffusion tensor collinear with the structural tensor) to balance new contrast with available SNR. We do not explicitly separate tubular and vascular flow, which remains an ongoing challenge for advanced renal DWI; efforts using cardiac gating[39] or triexponential fitting[40] have strong potential in this regard but carry costs in scan time or sampling requirements.

In addition to elucidating the microstructural and microvascular phenomena underlying renal dysfunction, this approach has future potential applications in predicting renal function outcomes postnephrectomy. One recent study showed significant postpartial-nephrectomy changes in IVIM parameters for both ipsilateral and contralateral kidneys, as well as positive correlations between ADC/IVIM parameters and eGFR.[34] This predictive application, requiring further recruitment and follow-up, is beyond the scope of the current work.

In conclusion, REFMAP-MRI analysis provides additional unique information with regard to renal dysfunction. Reproducibility analysis identified a subset of robust parameters for clinical use. In patients with known renal masses, directional changes in flow were noted which were not identified with IVIM analysis alone. This complex response demonstrates the need for the multilevel view provided by combined IVIM-DTI analysis, and the potential of this protocol to provide information about renal dysfunction which is distinct from that offered by eGFR alone. This approach may also have clinical utility in predicting renal response to surgical insult.

Acknowledgment

Contract grant sponsor: Center for Advanced Imaging Innovation and Research (CAI^{2}R; www.cai2r.net), NIBIB Biomedical Technology Resource Center; contract grant number: NIH P41 EB017183

We thank Mary Bruno, RT, and David Mossa, RT, for assistance in some image acquisitions.

Conflict of Interest

Thorsten Feiweier is an employee of Siemens Healthcare GmbH, owns stocks of Siemens AG, and holds patents filed by Siemens.

References

1. Centers for Disease Control and Prevention. Age-Adjusted prevalence of CKD Stages 1-4 by Gender 1999–2012. Chronic Kidney Disease (CKD) Surveillance Project; 2016.
2. Beben T, Rifkin DE. GFR estimating equations and liver disease. Adv Chronic Didney Dis 2015;22:337–342.
3. Prigent A. Monitoring renal function and limitations of renal function tests. Semin Nucl Med 2008;38:32–46.
4. Ibrahim H, Mondress M, Tello A, Fan Y, Koopmeiners J, Thomas W. An alternative formula to the Cockcroft-Gault and the modification of diet in renal diseases formulas in predicting GFR in individuals with type 1 diabetes. J Am Soc Nephrol 2005;16:1051–1060.
5. Elicker BM, Cypel YS, Weinreb JC. IV contrast administration for CT: a survey of practices for the screening and prevention of contrast nephropathy. AJR Am J Roentegenol 2006;186:1651–1658.
6. Winter KS, Helck AD, Ingrisch M, et al. Dynamic contrast-enhanced magnetic resonance imaging assessment of kidney function and renal masses: single slice versus whole organ/tumor. Invest Radiol 2014;49:720–727.
7. Zhang JL, Rusinek H, Bokacheva L, et al. Functional assessment of the kidney from magnetic resonance and computed tomography renography: impulse retention approach to a multicompartment model. Magn Reson Med 2008;59:278–288.
8. Kaewlai R, Abujudeh H. Nephrogenic systemic fibrosis. AJR Am J Roentegenol 2012;199:W17–23.
9. Huang WC, Levey AS, Serio AM, et al. Chronic kidney disease after nephrectomy in patients with renal cortical tumours: a retrospective cohort study. Lancet Oncol 2006;7:735–740.
10. Sigmund EE, Vivier PH, Sui D, et al. Intravoxel incoherent motion and diffusion-tensor imaging in renal tissue under hydration and furosemide flow challenges. Radiology 2012;263:758–769.
11. Le Bihan D, Breton E, Lallemand D, Grenier P, Cabanis E, Laval-Jeantet M. MR imaging of intravoxel incoherent motions: application to diffusion and perfusion in neurologic disorders. Radiology 1986;161:401–407.
12. Eisenberger U, Thoeny HC, Binser T, et al. Evaluation of renal allograft function early after transplantation with diffusion-weighted MR imaging. Eur Radiol 2010;20:1374–1383.
13. Rheinheimer S, Stieltjes B, Schneider F, et al. Investigation of renal lesions by diffusion-weighted magnetic resonance imaging applying intravoxel incoherent motion-derived parameters—initial experience. Eur J Radiol 2012;81:e310–316.
14. Chandarana H, Kang SK, Wong S, et al. Diffusion-weighted intravoxel incoherent motion imaging of renal tumors with histopathologic correlation. Invest Radiol 2012;47:688–696.
15. Basser PJ. Inferring microstructural features and the physiological state of tissues from diffusion-weighted images. NMR Biomed 1995;8:333–344.
16. Fukuda Y, Ohashi I, Hanafusa K, et al. Anisotropic diffusion in kidney: Apparent diffusion coefficient measurements for clinical use. J Magn Reson Imaging 2000;11:156–160.
17. Ries M, Jones RA, Basseau F, Moonen CTW, Grenier N. Diffusion tensor MRI of the human kidney. J Magn Reson Imaging 2001;14:42–49.
18. Lu L, Sedor JR, Gulani V, et al. Use of diffusion tensor MRI to identify early changes in diabetic nephropathy. Am J Nephrol 2011;34:476–482.
19. Hueper K, Gutberlet M, Rodt T, et al. Diffusion tensor imaging and tractography for assessment of renal allograft dysfunction-initial results. Eur Radiol 2011;21:2427–2433.
20. Lanzman RS, Ljimani A, Pentang G, et al. Kidney transplant: functional assessment with diffusion-tensor MR imaging at 3T. Radiology 2013; 266:218–225.
21. Cheung JS, Fan SJ, Chow AM, Zhang J, Man K, Wu EX. Diffusion tensor imaging of renal ischemia reperfusion injury in an experimental model. NMR Biomed 2010;23:496–502.
22. Gaudiano C, Clementi V, Busato F, et al. Diffusion tensor imaging and tractography of the kidneys: assessment of chronic parenchymal diseases. Eur Radiol 2013;23:1678–1685.
23. Notohamiprodjo M, Chandarana H, Mikheev A, et al. Combined intravoxel incoherent motion and diffusion tensor imaging of renal diffusion and flow anisotropy. Magn Reson Med 2015;73:1526–1532.
24. Ye Q, Chen Z, Zhao Y, et al. Initial experience of generalized intravoxel incoherent motion imaging and diffusion tensor imaging (GIVIM-DTI) in healthy subjects. J Magn Reson Imaging 2016;44:732–738.
25. Hilbert F, Bock M, Neubauer H, et al. An intravoxel oriented flow model for diffusion-weighted imaging of the kidney. NMR Biomed 2016;29:1403–1413.
26. Feiweier T. Bipolar diffusion encoding with implicit spoiling of undesired coherence pathways. In: Proc 19th Annual Meeting ISMRM, Montreal; 2011.
27. Patel J, Sigmund EE, Rusinek H, Oei M, Babb JS, Taouli B. Diagnosis of cirrhosis with intravoxel incoherent motion diffusion MRI and dynamic contrast-enhanced MRI alone and in combination: preliminary experience. J Magn Reson Imaging 2010;31:589–600.
28. NEMA. Determination of signal-to-noise ratio (SNR) in diagnostic magnetic resonance imaging. Methods of measurement. Volume MS 1-2008. Rosslyn, VA: National Electrical Manufacturers Association; 2008. p 17.
29. Hagmann P, Jonasson L, Maeder P, Thiran JP, Wedeen VJ, Meuli R. Understanding diffusion MR imaging techniques: From scalar diffusion-weighted imaging to diffusion tensor imaging and beyond. Radiographics 2006;26:S205–U219.
30. Jones DK, Basser PJ. "Squashing peanuts and smashing pumpkins": How noise distorts diffusion-weighted MR data. Magn Reson Med 2004;52:979–993.
31. Hirsch JG, Schwenk SM, Rossmanith C, Hennerici MG, Gass A. Deviations from the diffusion tensor model as revealed by contour plot visualization using high angular resolution diffusion-weighted imaging (HARDI). Magn Reson Mater Phys 2003;16:93–102.
32. Uppot RN, Sahani DV, Hahn PF, Gervais D, Mueller PR. Impact of obesity on medical imaging and image-guided intervention. Am J Roentegenol 2007;188:433–440.
33. Blondin D, Lanzman RS, Klasen J, et al. Diffusion-attenuated MRI signal of renal allografts: comparison of two different statistical models. AJR Am J Roentegenol 2011;196:W701–705.
34. Schneider MJ, Dietrich O, Ingrisch M, et al. Intravoxel incoherent motion magnetic resonance imaging in partially nephrectomized kidneys. Invest Radiol 2016;51:323–330.
35. Xu Y, Wang X, Jiang X. Relationship between the renal apparent diffusion coefficient and glomerular filtration rate: preliminary experience. J Magn Reson Imaging 2007;26:678–681.
36. Thoeny HC, De Keyzer F, Oyen RH, Peeters RR. Diffusion-weighted MR imaging of kidneys in healthy volunteers and patients with parenchymal diseases: initial experience. Radiology 2005;235:911–917.
37. Weis SM, Cheresh DA. Tumor angiogenesis: molecular pathways and therapeutic targets. Nat Med 2011;17:1359–1370.
38. Fellegara G, Rosai J. Multifocal capillary hemangioma-like vascular proliferation of the kidney associated with clear cell renal cell carcinoma: a case report and review of the literature. Int J Surg Pathol 2013;21:424–426.
39. Wittsack HJ, Lanzman RS, Quentin M, et al. Temporally resolved electrocardiogram-triggered diffusion-weighted imaging of the human kidney: correlation between intravoxel incoherent motion parameters and renal blood flow at different time points of the cardiac cycle. Invest Radiol 2012;47:226–230.
40. van Baalen S, Leemans A, Dik P, Lilien MR, >Ten Haken B, Froeling M. Intravoxel incoherent motion modeling in the kidneys: Comparison of mono-, bi-, and triexponential fit. J Magn Reson Imaging 2017;46: 228–239.